Predictive Synthesis of Freeform Carbon Nanotube Microarchitectures by Strain-Engineered Chemical Vapor Deposition

Sei Jin Park, Hangbo Zhao, Sanha Kim, Michael De Volder, and A. John Hart*

1. Introduction

3D structuring of surfaces at the micro- and nanoscales enables manipulation of electromagnetic waves, [1–4] mimicking of wetting and self-cleaning surfaces found in nature, [5,6]tailoring of structural color, [7–12] and design of novel mechanical properties. [13–15] To further design and scale these novel properties, high-throughput fabrication methods that achieve deterministic structuring of surfaces are needed. Each method may be classified by its range of achievable length scales, material capabilities, throughput, and achievable geometries. [16] One example is the realization of high-throughput fabrication of microstructured surfaces with multi-directional, re-entrant, or otherwise curved features is becoming increasingly important for applications such as phase change heat transfer, adhesive gripping, and control of electromagnetic waves. Toward this goal, curved microstructures of aligned carbon nanotubes (CNTs) can be fabricated by engineered variation of the CNT growth rate within each microstructure, for example by patterning of the CNT growth catalyst partially upon a layer which retards the CNT growth rate. This study develops a finite-element simulation framework for predictive synthesis of complex CNT microarchitectures by this strain-engineered growth process. The simulation is informed by parametric measurements of the CNT growth kinetics, and the anisotropic mechanical properties of the CNTs, and predicts the shape of CNT microstructures with impressive fidelity. Moreover, the simulation calculates the internal stress distribution that results from extreme deformation of the CNT structures during growth, and shows that delamination of the interface between the differentially growing segments occurs at a critical shear stress. Guided by these insights, experiments are performed to study the time- and geometry-depended stress development, and it is demonstrated that corrugating the interface between the segments of each microstructure mitigates the interface failure. This study presents a methodology for 3D microstructure design based on “pixels” that prescribe directionality to the resulting microstructure, and show that this framework enables the predictive synthesis of more complex architectures including twisted and truss-like forms. Carbon Nanotubes surfaces with inclined elements, namely micro- or nanoscale posts that are tilted or curved in a desired direction, which for instance can be achieved by inclined polymerization, [17]lithography, [18] or etching [19,20] techniques. Vertical post arrays can be bent by inducing a strain gradient by inclined electron beam deposition of metal films in conjunction with strain induced by elastocapillary densification, [21] thermal expansion mismatch, [22] or oblique electron beam irradiation. [23] While impressive, these techniques are typically limited to pillar arrays all bending in the same direction. On the other hand, direct-write methods such as focused ion beam and multi-photon lithography [24] can produce more complex curved, overhanging, and twisted micro- and nanostructures; [25] however, their throughput is inadequate for large scale production. In general, there is a trade-off between the complexity of structures and the throughput of the production technique. This motivates the need for a scalable fabrication technique where individual structures can be shaped independently, achieving complete heterogeneity of resulting structures by design. We have recently demonstrated

a manufacturing technique for freeform carbon nanotube (CNT) microstructures, where planar catalyst patterns are designed to specify the local upward growth rate and collective curvature of the CNTs within each microstructure. [26] This method is attractive to the above motivation because the vertical growth rate of the CNTs is rapid (typically 10–100 μm min −1 or greater), and because CNTs can be produced by planar patterning of the catalyst in combination with atmospheric pressure chemical vapor deposition (CVD), on a variety of substrates. [27–29] However, to fully realize the potential of this method, a predictive approach is needed whereby the shape of the CNT microstructures can be predicted by design, rather than by iterative experimentation. In this paper, we enable such a predictive synthesis approach for complex CNT microstructures. We construct a step-wise finite element simulation of the strain-engineered CNT forming process, which is informed by measurements of the relative growth rates determined by substrate patterning, along with the anisotropic mechanical properties of the CNT forests. This framework also allows us to investigate the magnitude and distribution of internal stresses within the growing CNT structures, and develop practical design strategies to mitigate mechanical failure of the structures due to the forces involved in synthesis. Finally, the applicability of the model to complex surface designs is showcased by simulating the formation of CNT microstructures with multi-directional curved trajectories.

2. Results and Discussion

Spatial control of the growth rate of CNTs is achieved by selectively patterning the supported catalyst (Fe/Al 2O3) on a secondary TiN layer (see Experimental Section). In areas where the catalyst is placed on TiN, the CNT forest growth rate is reduced. Therefore, patterning of catalyst features that partially overlap TiN features causes formation of a curved CNT microstructure due to mechanical coupling between the CNTs at the interface between the differentially growing segments. In contrast to straight vertical CNT microstructures (Figure 1a), the curved structures (Figure 1b) exhibit a distinct interface along the boundary between the underlying growth pattern, and in some cases the structures split along the interface as growth proceeds. To establish a predictive model of the CNT formation process, we treat the differentially growing CNT segments as having independently defined growth rates and mechanical properties. The shape evolution of the CNT microstructures during growth is therefore governed by the time-dependent growth rates of each portion of a microstructure, their mechanical properties, and the boundary conditions acting upon each segment.

2.1. Growth Simulation Scheme

The simulation scheme (Figure 2) discretizes the CNT growth into timesteps; at each step, a new material layer is added at the base of the microstructure, i.e., the interface between the previously grown CNTs and the substrate. The cross-section of exemplary rectangular structures having catalyst area, A, with a fraction of TiN layer overlap, O, is first designated in two adjacent segments, O × A, and(1 − O) × A, representing the CNT forest areas that will emerge at different upward growth rates. At the beginning of each growth step, a single planar layer of finite elements is inserted at the interface between the base of the CNT structure and the rigid substrate; the element heights are proportional to the growth rate of the segment. The nodes on the bottom surface are then relieved of all constrained degrees of freedom and those at the new base are fixed. For each new layer, an initial compressive stress state is assigned to the faster-growing portion (catalyst on SiO 2) such that, if unconstrained, it would expand by an amount proportional to the measured relative growth rate, RRel = RTiN/RSiO2.Here, RTiN and RSiO2 are the instantaneous vertical growth rates of CNTs from catalyst placed on TiN/SiO 2 and SiO 2respectively. The structure deforms incrementally after each growth-relaxation step, and iteration through a series of steps simulates the coupled growth-deformation pro-cess. While this approach abstracts the complex dynamics of CNT self-organization

and morphology evolution, we show later that it provides a highly accurate prediction of the final form of CNT microstructures. The stress states and elemental orientations are conserved between steps, and in the nominal simulations the vertical step size is 1 μm, corresponding to ≈1 s of CNT growth in the experimental process. The stiffness matrix for the finite elements is constructed using measured property data, and the material properties were assumed to be linear as discussed later. This scheme was implemented using a commercial finite element method (FEM) software package (Ansys Mechanical APDL 14.5). A similar modelling scheme has been applied to explore tip growth of plant cells [30] where a turgor presure was applied to the tubular cell tip, and the model was solved for displacements then re-meshed to accommodate addition of cellular matter.

2.2. CNT Growth Kinetics and Mechanical Properties

To accurately inform the strain-engineered CNT growth model, we fi rst studied the growth kinetics and the mechanical properties of CNTs grown from the Fe/Al 2O3/SiO2 andFe/Al 2O3/TiN/SiO2 substrates. Figure 3 shows the measured relationships among CNT forest height and the most critical process parameters: CNT growth time (up to 5 min), growth temperature (755, 770, 785, 800 °C), duration of annealing prior to CNT growth (10, 30 min), and TiN underlayer thick-ness (none, 50, 100 nm). The presence of the TiN underlayer influences the morphology and activity of the catalyst, and is found to result in slightly smaller diameter CNTs having a lower collective growth rate, [26,31] without a discernible difference in CNT density. Therefore, the annealing duration and underlayer thickness were expected to also have an important influence on the CNT growth kinetics. As shown in Figure 3, the effective CNT growth rate (quantified based on the CNT forest height after 5 min of growth) is higher on SiO 2 than on TiN underlayers of 50 and 100 nm. The growth rate also increases with temperature for CNTs on SiO 2, but for CNTs grown on TiN, the growth rate reaches a maximum at 785 °C and then decreases at higher temperatures. The relative CNT growth rates (Rrel .)after 10 and 30 min of catalyst annealing times are shown in Figure 3b,c respectively. For both recipes, the relative growth rate is inversely related to the TiN underlayer thickness (up to the 100 nm maximum thickness tested). Moreover, the growth rate of CNTs changes with time (Figure S2, Supporting Information); the CNT height increases almost linearly up to 10 min of growth time, and afterward, the CNT height does not increase indicating that the growth has terminated. This limits the height of the CNT structures that can be grown using this technique to ≈1300 μm. small 2016, 12, No. 32, 4393–4403Figure 1. Catalyst pattern design and exemplary results for vertical and curved (strain-engineered) CNT microstructure growth. a) From left to right: standard catalyst microfeature design, optical microscope image of catalyst (Fe/Al 2O3) on SiO2/Si substrate, SEM image of resulting carbon nanotube microstructures vertically grown from the substrate by chemical vapor deposition, and high magnification SEM image of CNTs within the microstructure. b) From left to right: multi-layer offset pattern of catalyst and TiN underlayer, optical microscope image of offset pattern, SEM image of curved CNT micropillar grown from this pattern, and high magnification SEM image of CNTs near the SiO 2/TiN interface. SEM images of large arrays of structures in (c) and (d) are shown to highlight their uniformity.

To complete the inputs to the model, we next quantified the mechanical properties of the CNT forests grown from catalyst on SiO 2, TiN (50 nm) and TiN (100 nm) layers. A CNT forest can be idealized as a transversely isotropic material where the CNTs are parallel to the y-axis, perpendicular to the substrate, and the plane of isotropy (xz) is parallel to the substrate. Therefore, for each portion of the microstructure, the fi ve independent material properties of interest are the elastic moduli (E x, E y), shear modulus (G zx)and Poisson's ratios (ν xy, ν zx). Uniaxial compression tests were performed on CNT microstructures grown on Fe/Al 2O3/SiO2 and Fe/Al 2O3/SiO2/TiN (100 nm). Knowing that the compression behavior of CNT forests under small strains allows

approximation as an open cell foam, [32] the unloading slope of the stress–strain curve was used to calculate the modulus in the normal direction (E y). We chose to characterize CNT microstructures grown at 800 °C because this growth temperature showed the greatest difference in growth rates between the two cases, and therefore enabled the most extreme deformations when the differentially growing segments were coupled. In this case, the CNTs on Fe/Al 2O3/SiO2 had E y = 297 ± 101 MPa, and the CNT forest on Fe/Al 2O3/SiO2/TiN had E y = 496 ± 49 MPa. Here, the variation represents one standard deviation of a population of measurements, and arises due to spatial and run-to-run CNT density variations. This measured elastic modulus and a linear elastic relationship are valid within approximately 5% global compressive strain of the CNT forest, beyond which local buckling of the CNTs occurs. [33] From this point, understanding from previous work was applied to estimate the additional elastic constants of interest, giving the full set of values listed in Table S1 in the Supporting Information. The anisotropy ratio of 10 was assumed (E x = E y/10) for the CNT forest; [34,35] this assumption was not verified by direct measurement, but the modulus anisotropy was not found to significantly affect the simulation results as shown in Figure S3 in the Supporting Information. In previous work, the shear modulus, G xy (= G yz), of the CNT forests grown on Fe/Al 2O3/SiO2 has been measured to be 1.0–13.3 MPa; [35–37] therefore, we also specified G xy = E y/10.The Poisson's ratio of CNT microstructures is assumed to be zero in all directions. [38] G zx was calculated from transverse isotropy relation, G zx = E z/2(1+ ν zx).

2.3. Geometric Comparison of Experiments and Simulations

The simulation allows us to visualize the shape evolution of CNT microstructures during growth (Video S1, Supporting Information), and explore the distribution of stress and strain arising due to the differential growth. First, within each microstructure, we find the CNTs that nominally grow at a slower rate (i.e., Fe/Al 2O3/TiN/SiO2) are in tension near the interface, and the CNTs that nominally grow faster (i.e., Fe/Al 2O3/SiO2) are in compression. This results in a large stress gradient spanning the interface, and a maximum shear stress at the interface. Therefore, the interface would be the most likely location of shear failure of the micro-structure, either as the microstructure grows, or when the structure is loaded. [26] By examining the SEM image of a curved CNT microstructure (Figure 4a) we see that the axial compressive stresses cause local buckling of CNTs near the interface toward the bottom of the microstructure (Figure 4b), and the shear stress causes separation near the tip of the microstructure (Figure 4c, Figure S4, Supporting Information). Next, we simulated growth of curved CNT micropillars from square catalyst patterns with varying overlap with the TiN underlayer (Figure 5). First, we note that the location of maximum shear stress in the final simulation step coincides with the location of interface failure in the fabricated CNT structures. As a measure of the accuracy of the simulation, the normalized position of the far corner ("tip") that bends away from the base of the microstructure was calculated. By this metric (Figure 6a), compared for square CNT micropillars with 40 × 40 μm 2 square cross-sections, we fi nd that maximum tip position in the x-axis is achieved when the differentially growing regions are equal in size. The stepwise growth model achieves excellent agreement with measurements of the series of structures imaged by SEM, whereas a simple bimetallic strip model [26] significantly underestimates the magnitude of displacement. Also, as the amount of catalyst pattern overlap on TiN increases, the fi nal height of the structures decreases, because a greater portion of the CNTs is growing at a slower average rate. A further series of simulations and experiments was performed to assess the influence of growth temperature on tip position (Figure S5, Supporting Information), and in all cases the final values matched within 16%. Yet a more accurate validation of the model is made by comparing the edge profile of individual CNT micropillars measured by edge detection (ImageJ, NIH), to the positions of the nodes from the simulation. Here, simulations were performed at a series of constant relative growth rates (Figure 6b); in all cases, the local radius of curvature increases from the tip to the base,

and the overall radius of curvature is inversely related to the relative growth rate. The closest agreement occurs at a relative growth rate of 0.50, as expected from the direct growth rate measurements at this condition (Figure 2c, 100 nm TiN, 800 °C). The deviation between the predicted and measured profiles is also primarily influenced by the time variation of CNT growth rate (Figure S2b, Sup-porting Information); therefore, improved prediction of the edge profile is achieved with simulations where the growth rate decreases linearly with time (from 0.53 to 0.50, Figure 6c).

2.4. Mitigating Interface Failure

The high shear stresses at the internal interface can cause splitting of the compound microstructure, which in turn influences the fidelity of the formed shape. The sustenance of a large stress gradient at the interface between the differentially growing portions suggests there is a continuous CNT network at the interface, whose integrity is governed by the entanglement and adhesive forces among CNTs. We observed above that interface failure in the simple bending structures occurs at the predicted location of maximum shear stress; however, the coupling between growth, stress, and deformation prevents us from using these structures to extract a more general finding as to the relationship between local stress and interface failure. Consequently, an array of “checkerboard” catalyst pat-terns was designed to investigate the origin and mitigation of interface failure. In each checkerboard pattern, the total area of CNTs (i.e., catalyst pattern area) is the same, yet the interfacial area between segments on TiN and SiO 2/TiN is varied by incrementing the number of divisions of the checkerboard, n, giving 2 n squares in each series. Synthesis of CNT forests from these patterns (Figure 7a), at a series of temperatures, led us to observe that interface failure is observed at higher temperatures (where there is a greater difference in CNT growth rate between adjacent squares within each board), and/or for checkerboard patterns with lesser n (i.e., having greater interfacial stress). Simulation of identical checkerboards verified this intuition, and allowed us to approximate a maximum shear strain (defined as the maximum shear stress divided by the shear modulus) for each checkerboard (Figure 7b,c). Comparing to experiment, all structures showing interface failure have a maximum shear stress exceeding ≈12 MPa; therefore, we conclude that interface failure can be prevented by selecting the CNT growth conditions such that the maximum shear stress does not exceed this critical value. These findings also raise the interesting question as to how the mechanical competition between the coupled CNT segments influences the CNT growth process itself. It is known that CNT forest growth can exert significant forces, which have been approximated by performing CNT growth under static weights, [39] or acting against compliant mechanisms. [40] This force output capability of CNT growth is essential to create the curved microstructures, and is found in some cases to exceed the interfacial strength along the internal boundaries. Moreover, stress can also influence the CNT alignment, as seen by examining the CNTs especially near the interface. Therefore, while our simulation captures how the elastic properties of the CNT forests and their nominal growth kinetics influence the stress distribution above the substrate, there is, in turn, a non-uniform stress exerted on the substrate where the catalyst resides. Consequently, we expect there is mechanochemical feedback at play in determining the local topology of the CNT network as it is formed at the base of the structure. In fact, we observe that the apparent CNT growth rate is affected by stresses exerted during growth, because the fi nal height of CNT structures grown on the checkerboard patterns is between the limiting cases of growth on Fe/Al 2O3/SiO2 or Fe/Al 2O3/TiN/SiO2(Figure S6, Supporting Information).

2.5. Predictive Synthesis of CNT Microarchitectures

Using the simulation routine along with parametric knowledge of the differential growth behavior, it is possible to accurately predict the 3D CNT shape that will be formed, and identify limitations of the process; we refer to this approach as “predictive synthesis”. For the exemplary case of curved

micropillars, we show in Figure 8 the results of a para-metric series of simulations spanning relative growth rate (i.e., growth temperature) and growth time. Here, the final tip position is reported as the output metric; the boundary with the region marked “not feasible” represents structures whose tip intersects the substrate, thereby completing an arch shape. Therefore, with the knowledge of shear strength of the CNT interface between the differentially growing portions, it is possible to predict a set of geometries and CNT growth parameters that will produce structures that do not fail at the interface (Figure 8c). We can also tailor the interface to reduce the local shear stress. We demonstrate this in CNT micropillars where the substrate is patterned with a fractal-like corrugated interface, denoted by an interface complexity index (ICI) that was previously used in study of the mechanics of skeletal suture joints. [41] Using this approach, we fabricated CNT micropillars that curve without interface failure (Figure 9). Last, the capability to tailor the local growth rate and ensuing curvature of CNT microstructures allows us to design and simulate the formation of more complex micro-architectures. Conceptually, any composite catalyst pat-tern can be constructed starting from the most basic “pixel” element, which is a square catalyst feature partially overlap-ping SiO 2 and a growth retarding layer such as TiN. The CNT microstructure grown from this element will curve toward the side that overlaps the TiN layer. Variations of these elements can be derived by one or more successive operations; such as varying the catalyst/TiN layer overlap, or elongating and/or scaling the element (Figure 10a). Complex geometries can be built by merging multiple regions of differentially growing CNT pixels. For example, in Figure 10b a semicircular CNT microstructure designed to curve outward, a cross pattern designed to twist in the clock-wise direction, and the pattern for a cluster of micropillars that meets at central point are shown. In Figure 10c, we com-pare the simulated and experimentally obtained structures, which show remarkable agreement. This result showcases the versatility of the predictive synthesis routine as a tool for designing new 3D surface architectures and reducing trial-and-error optimization. This high fidelity of prediction is achieved in spite of our specification of time-invariant CNT growth rates for each portion and linear anisotropic material behavior. Further, the CNT growth simulation cannot capture spatial variations and run-to-run fluctuations of CNT growth, [42] and potential effects of stress on the CNT growth kinetics and morphology. Also, the stress gradient between the CNT segments could be mitigated by deposition of the growth retarding TiN under-layer with a gradient thickness, or by employing grayscale patterning such that the CNT growth rate changes gradually across the structure. Use of time-variant CNT growth conditions that influence the relative rates, e.g., changing the temperature during CNT growth, could enable further versatility in tailoring the curvature of the CNT microstructures.

3. Conclusions

We have demonstrated the capability for predictive synthesis of freeform CNT microstructures, combining a novel strain-engineered growth technique with a step-wise finite element modelling approach that captures the anisotropic mechanics and growth kinetics of CNT forests. Although this approach abstracts the complex dynamics of CNT self-organization and morphology evolution, it is shown to predict the final form of CNT microstructures with impressive fidelity. Such a predictive tool can enable a priori design of substrate patterns and CNT growth parameters to achieve target shapes, and to mitigate limiting mechanisms such as interfacial shear failure. We envision a number of interesting ways to extend this work. First, more detailed quantitative characterization, such as by image analysis and/or 3D tomography, can extend our interpretation of the shape predictions and the underlying growth mechanics. Second, computationally efficient approaches could be used to seek desired 3D shapes using the growth simulations, without requiring complete simulation of the parameter space. Third, expansion of this framework to include relationships between geometry and material properties (e.g., stiffness, thermal conductivity), could enable predictive design for specific

applications, such as surfaces with engineered wettability, strong dry adhesion, and low contact resistance. Fourth, miniaturization of the strain-engineered growth technique to structures with critical dimensions in the ≈0.1–10 μm scale (Figure S7, Supporting Information) rather than the 10–100 μm scale would expand its applicability to surface engineering especially for optical and biomedical applications.

Acknowledgements: Financial support to S.P. and A.J.H., and for experimentation, was provided by the Air Force Office of Scientific Research Young Investigator Program (FA9550-11-1-0089), and the MIT Department of Mechanical Engineering (startup funds to A.J.H.). Financial support to S.K. was provided by the National Science Foundation (CMMI-1463344). Financial support to H.Z. was provided by the National Institutes of Health (1R21HL114011-01A1). M.D.V. acknowledges support from the ERC starting grant 337739-HIENA and the Marie Curie CIG Grant 618250-CANA. The authors thank Sameh Tawfick for discussions and contributions to earlier stages of this work, and Prof. Wei Lu and Prof. Anthony Waas of the University of Michigan for advice on modeling approaches. Microfabrication was performed at the Lurie Nanofabrication Facility (LNF) at the Univer-sity of Michigan, at the MIT Microsystems Technology Laboratory (MTL), and at imec (Heverlee, Belgium). Electron microscopy was performed at the Michigan Electron Microbeam Analysis Laboratory (EMAL), the MIT Center for Materials Science and Engineering (CMSE), and at imec. Nanoindentation was performed at the MIT NanoMechanical Technology Laboratory (Nanolab).

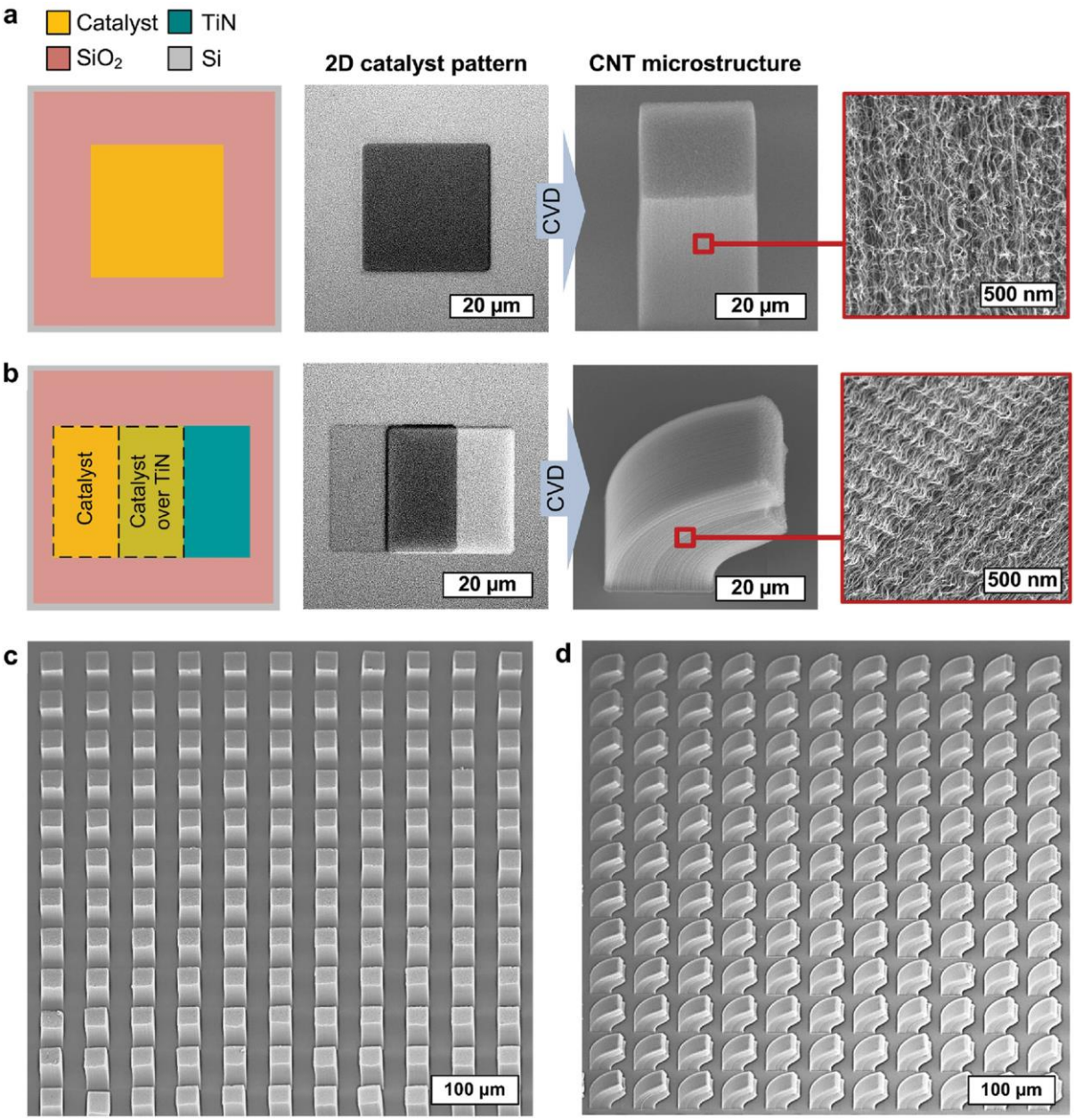

Figure 1. Catalyst pattern design and exemplary results for vertical and curved (strain-engineered) CNT microstructure growth. a) From left to right: standard catalyst microfeature design, optical microscope image of catalyst (Fe/Al_2O_3) on SiO_2/Si substrate, SEM image of resulting carbon nanotube microstructures vertically grown from the substrate by chemical vapor deposition, and high magnifi cation SEM image of CNTs within the microstructure. b) From left to right: multi-layer offset pattern of catalyst and TiN underlayer, optical microscope image of offset pattern, SEM image of curved CNT micropillar grown from this pattern, and high magnifi cation SEM image of CNTs near the SiO_2/TiN interface. SEM images of large arrays of structures in (c) and (d) are shown to highlight their uniformity.

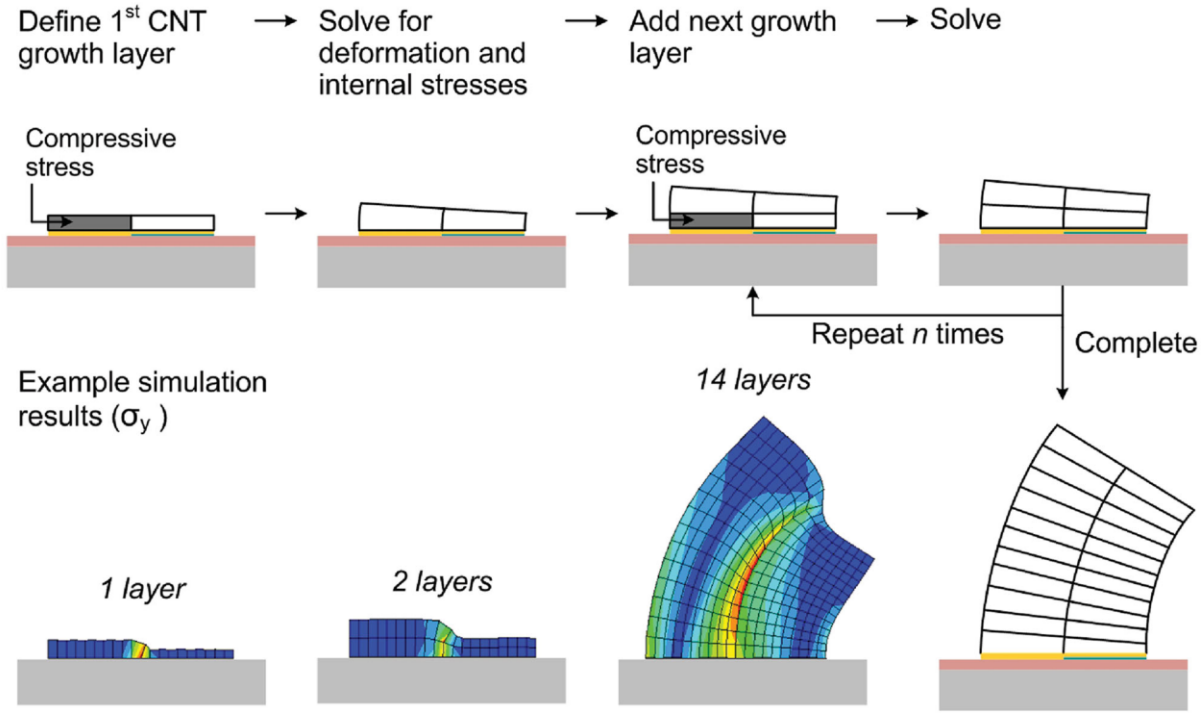

Figure 2. Finite element simulation scheme for strain-engineered CNT microstructure growth. The CNT growth process is discretized into layers where material is added at the bottom of the CNT microstructure. An example simulation model is shown along with the corresponding discretization for 14 layers.

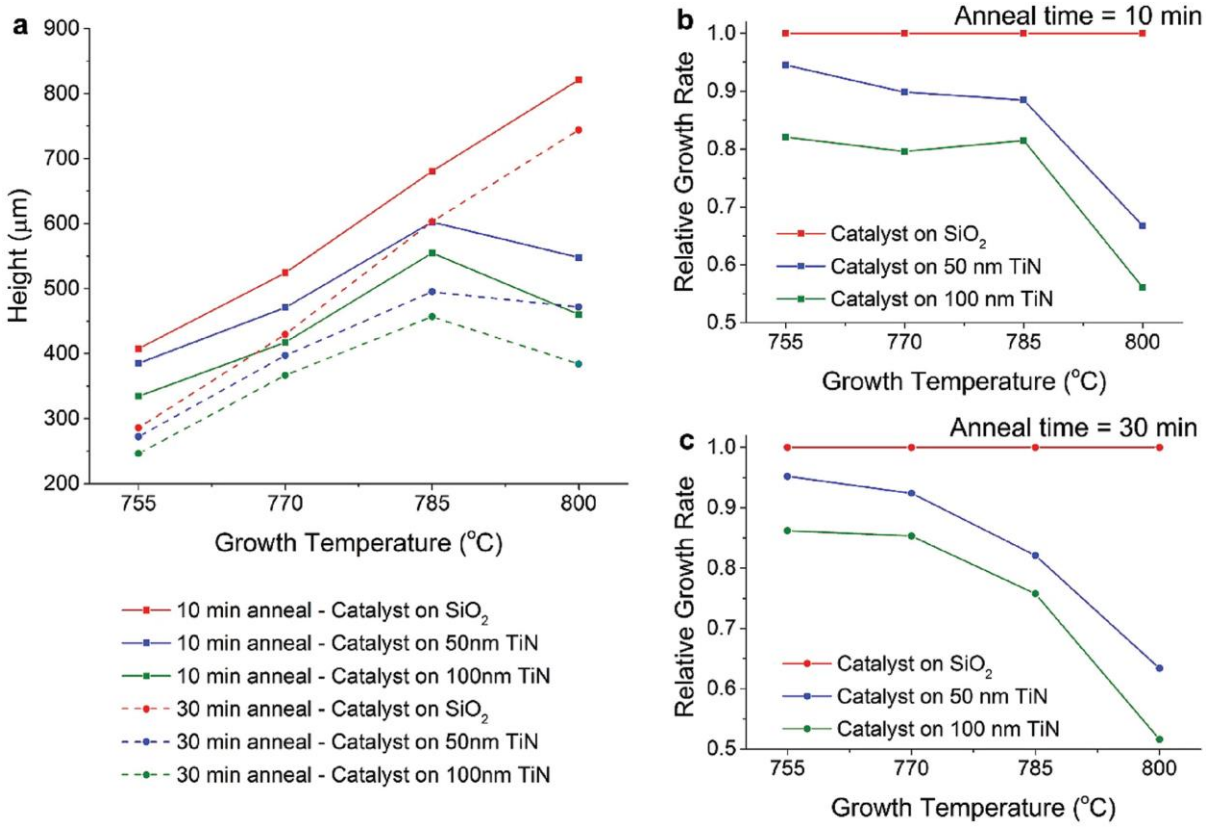

Figure 3. Control of relative CNT forest height grown from Fe/Al $_2$O $_3$ with optional TiN underlayer. a) Comparison between CNT heights on catalyst on SiO $_2$, 50 and 100 nm TiN. The CNT forests were grown at 755, 770, 785, and 800 °C for 5 min. Relative CNT growth rate on various catalyst stacks normalized to that of CNTs grown on catalyst on SiO $_2$, for b) 10 min of annealing in H $_2$/He before hydrocarbon exposure, and c) 30 min of annealing.

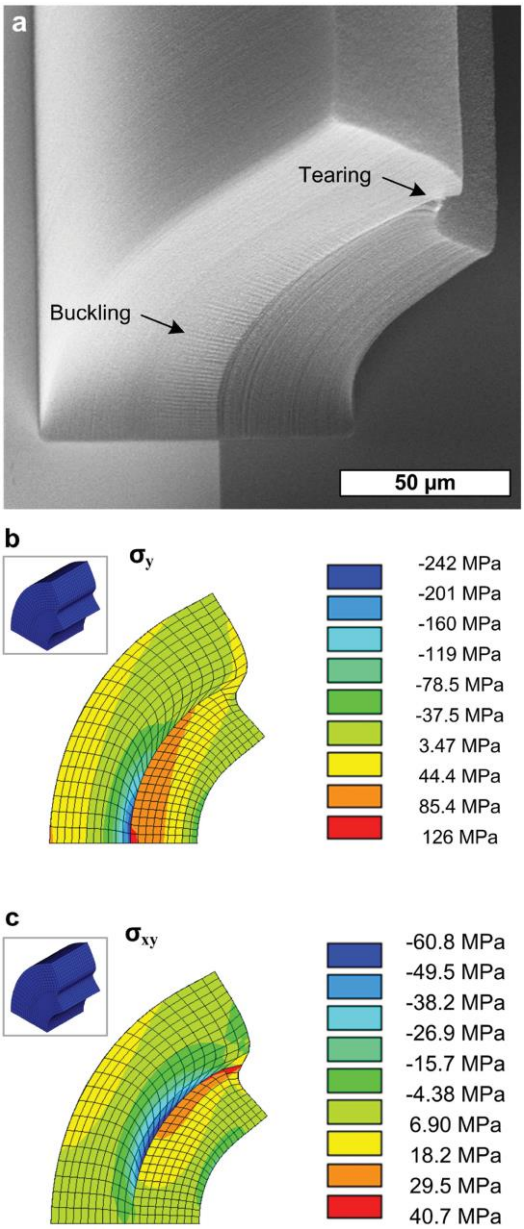

Figure 4. Exemplary comparison between curved CNT microstructure and stress fi elds predicted by FEM simulation. a) SEM image of CNT microstructure showing tearing at the top of the interface and local CNT buckling lower along the interface. b) FEM simulation of axial stress distribution, wherein the axis is locally tangent to the interface. The areas with greatest compressive stress match the areas where CNT buckling is observed in the SEM image. c) FEM simulation of shear stress, where maximum indicates location of tearing.

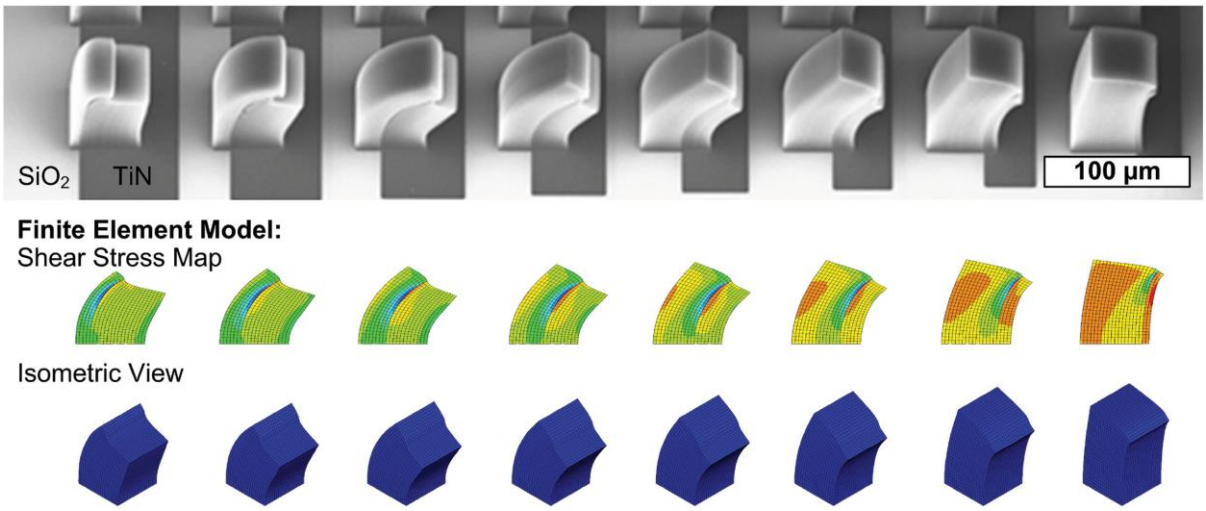

Figure 5. Visual comparison between series of curved CNT microstructures and results of FEM simulations, with varying catalyst-TiN overlap. Note that the internal interface of each structure splits near the predicted location of maximum shear stress.

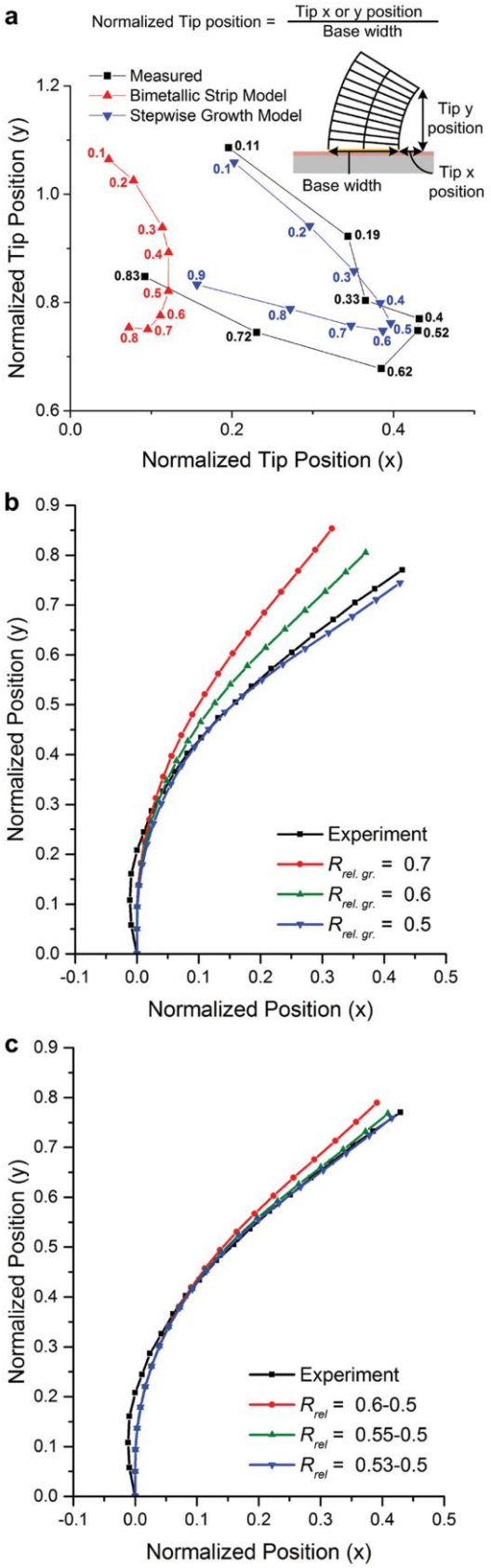

Figure 6. Evaluation of geometric accuracy of curved microstructure simulations. a) Normalized tip position (top right corner) of structures fabricated with different catalyst overlap area on TiN. Numbers next to datapoints indicate corresponding overlap values. b) Edge curves (from base along edge to tip as defi ned above) simulated with constant relative CNT growth rates. c) Edge curves simulated with linearly decreasing relative CNT growth rates.

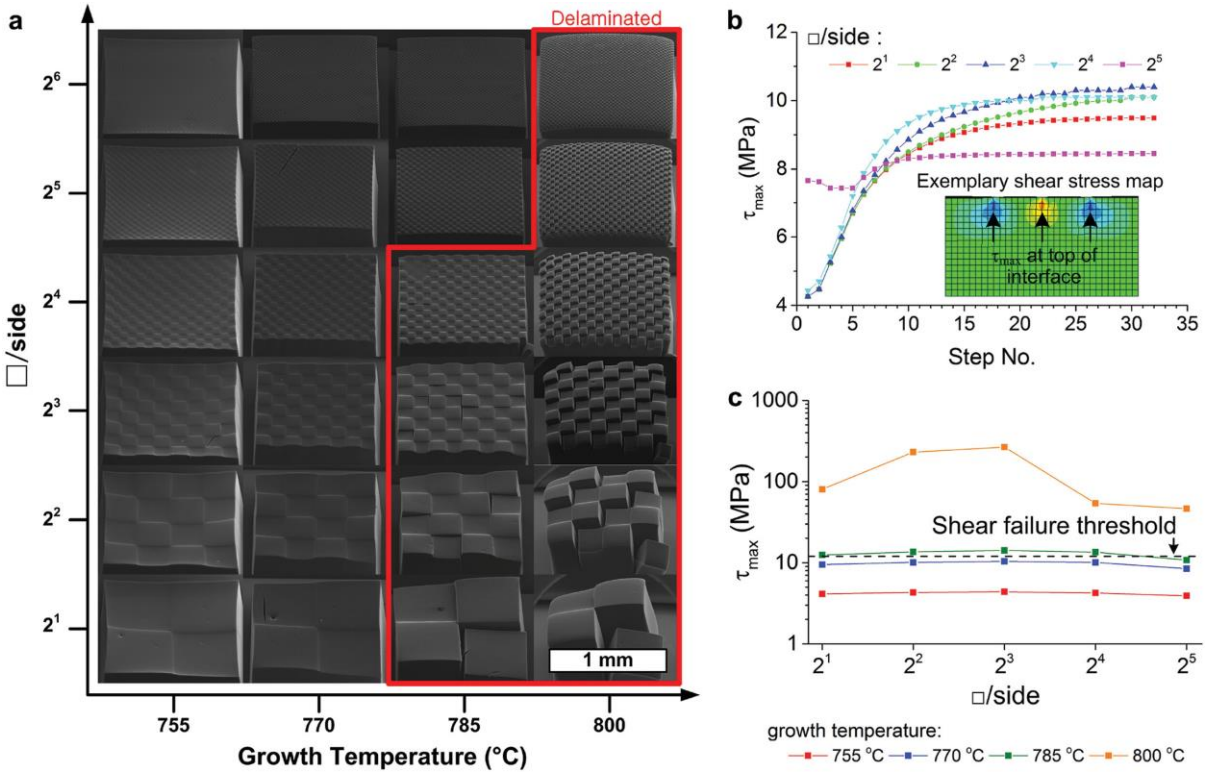

Figure 7. Use of “checkerboard” patterns to elucidate competition between stress exerted by differential growth, and interfacial strength of internal CNT forest interface. a) Arrays of patterns (each “board” 1 mm 2) produced at different synthesis temperatures, showing that interface failure is favored for low *n* and/or high temperature. b) Simulated relationship between maximum shear stress and simulation step at 770 °C growth temperature. c) Simulated relationship between maximum stress (after fi nal step) and number of divisions, identifying an approximate critical shear stress of 12 MPa, at which interface failure occurs between adjacent squares.

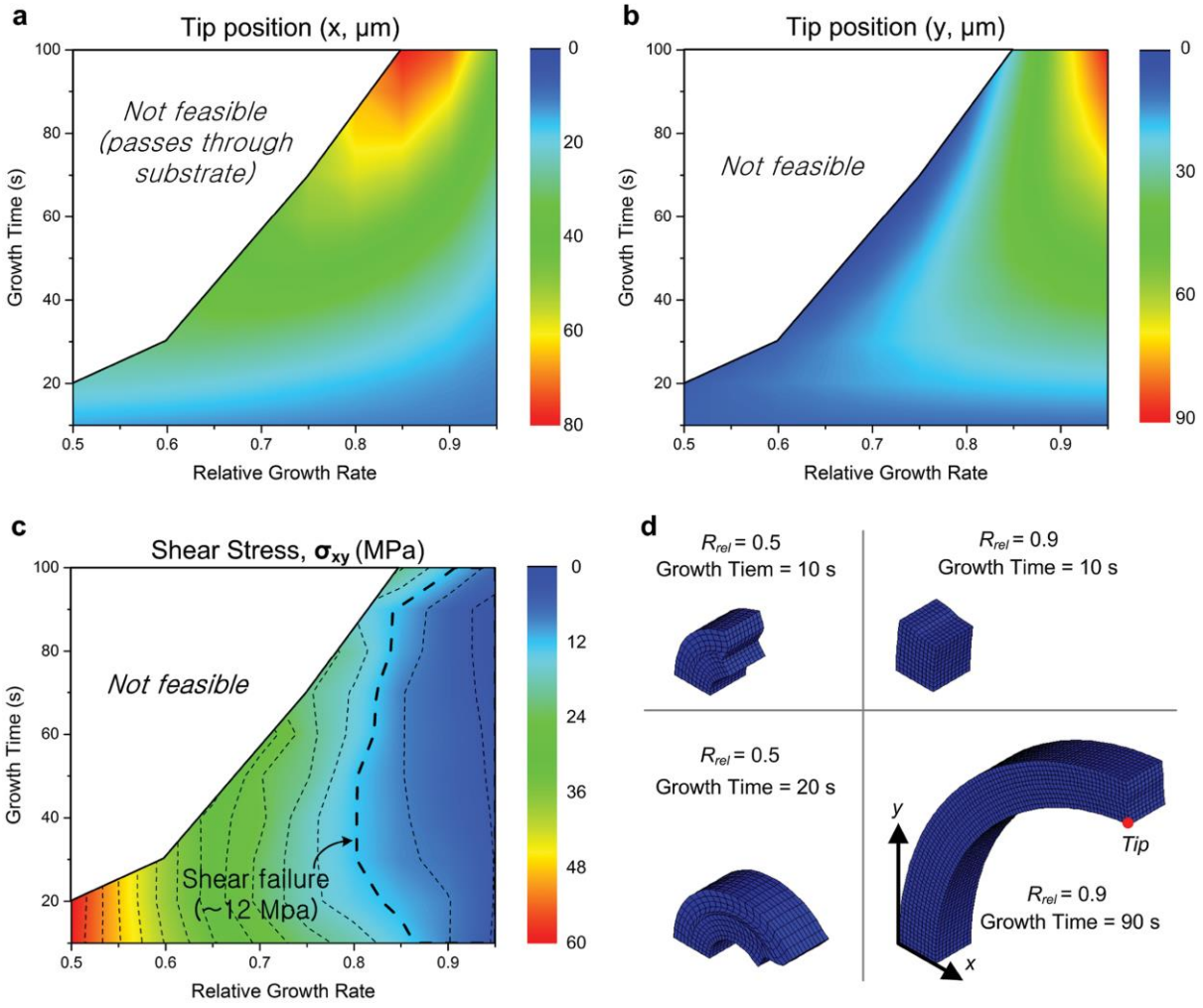

Figure 8. Parametric study of strain-engineered CNT growth of curved micropillars, as a demonstration of predictive synthesis to achieve a target geometry without exceeding the critical interfacial shear stress or intersecting with the substrate (“not feasible”). Simulations shown are for square (10 · 10 μm catalyst) CNT pillars with 50% catalyst overlap on TiN. Resultant tip position in (a) *x* - and (b) *y* - direction. c) Predicted maximum shear stress. d) Example predicted fi nal shapes.

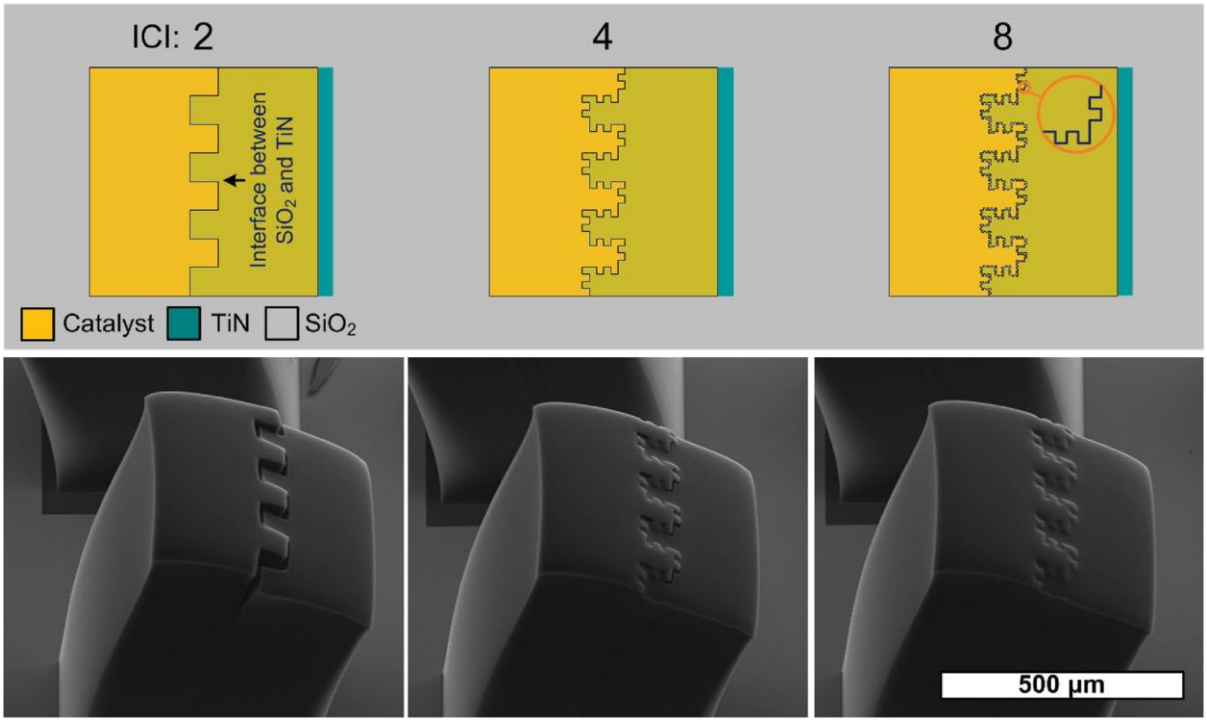

Figure 9. Use of a fractal interface design to increase the interfacial area and mitigate tearing.

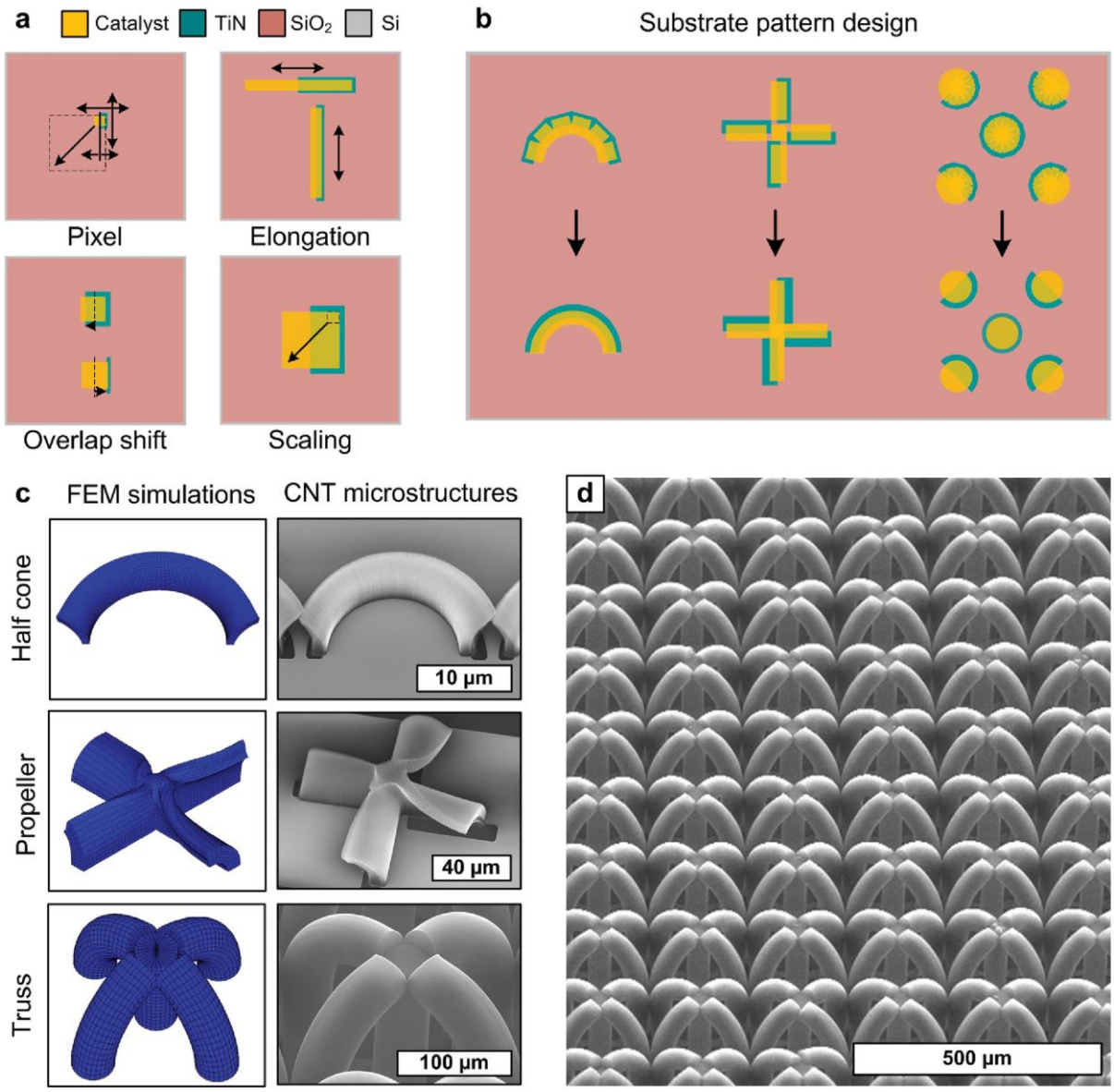

Figure 10. A conceptual strategy to "program" the formation of 3D CNT microarchitectures using compound catalyst/underlayer patterns. a) A single catalyst "pixel" can be elongated, shifted, and scaled. b) Compound shapes can be designed for multi-directional CNT architectures. c) The results of corresponding FEM simulations are compared to SEM images for the "half cone," "propeller," and a "microtruss." d) A large array of microtruss structures grown in a single CVD step on a Si substrate.

References

[1] J. B. Pendry, A. J. Holden, W. J. Stewart, I. Youngs, Phys. Rev. Lett.1996, 76, 4773.

[2] J. B. Pendry, A. J. Holden, D. J. Robbins, W. J. Stewart, IEEE Trans.1999, 47, 2075.

[3] D. R. Smith, W. J. Padilla, D. C. Vier, S. C. Nemat-Nasser, S. Schultz,Phys. Rev. Lett. 2000, 84, 4184.

[4] M. S. Kushwaha, P. Halevi, G. Martínez, L. Dobrzynski,B. Djafari-Rouhani, Phys. Rev. B 1994, 49, 2313.

[5] W. Barthlott, C. Neinhuis, Planta 1997, 202, 1.

[6] W. R. Hansen, K. Autumn, Proc. Natl. Acad. Sci. USA 2005, 102,385.

[7] P. Vukusic, J. R. Sambles, Nature 2003, 424, 852.

[8] J. Zi, X. Yu, Y. Li, X. Hu, C. Xu, X. Wang, X. Liu, R. Fu, Proc. Natl. Acad. Sci. 2003, 100, 12576.

[9] T. Tan, D. Wong, P. Lee, Opt. Express 2004, 12, 4847.

[10] P. Vukusic, B. Hallam, J. Noyes, Science 2007, 315, 348.

[11] R. A. Potyrailo, H. Ghiradella, A. Vertiatchikh, K. Dovidenko,J. R. Cournoyer, E. Olson, Nat. Photonics 2007, 1, 123.

[12] L. Feng, Y. Zhang, M. Li, Y. Zheng, W. Shen, L. Jiang, Langmuir2010, 26, 14885.

[13] N. A. Fleck, V. S. Deshpande, M. F. Ashby, Phys. Eng. Sci. 2010,466, 2495.

[14] B. Xu, F. Arias, S. T. Brittain, X. M. Zhao, B. Grzybowski,S. Torquato, G. M. Whitesides, Adv. Mater. 1999, 11, 1186.

[15] J. Meaud, T. Sain, B. Yeom, S. J. Park, A. B. Shoultz, G. Hulbert,Z.-D. Ma, N. A. Kotov, A. J. Hart, E. M. Arruda, A. M. Waas, ACS Nano 2014, 8, 3468.

[16] S. Tawfick, M. De Volder, D. Copic, S. J. Park, C. R. Oliver,E. S. Polsen, M. J. Roberts, A. J. Hart, Adv. Mater. 2012, 24, 1628.

[17] M. Han, W. Lee, S.-K. Lee, S. S. Lee, Sens. Actuators A: Physical2004, 111, 14.[18] M. M. Hawkeye, M. J. Brett, J. Vac. Sci. Amp Technol. A 2007, 25,1317.

[19] S. Takahashi, K. Suzuki, M. Okano, M. Imada, T. Nakamori, Y. Ota,K. Ishizaki, S. Noda, Nat. Mater. 2009, 8, 721.

[20] F. Hui, L. Xudong, S. Shuang, X. Ying, Z. Jing, Nanotechnology2008, 19, 255703.

[21] S. Tawfick, A. J. Hart, M. De Volder, Nanoscale 2012, 4, 3852.

[22] K.-H. Chu, R. Xiao, E. N. Wang, Nat. Mater. 2010, 9, 413.

[23] T.-i. Kim, H. E. Jeong, K. Y. Suh, H. H. Lee, Adv. Mater. 2009, 21, 2276.

[24] S. Maruo, O. Nakamura, S. Kawata, Opt. Lett. 1997, 22, 132.

[25] J. K. Gansel, M. Thiel, M. S. Rill, M. Decker, K. Bade, V. Saile,G. von Freymann, S. Linden, M. Wegener, Science 2009, 325, 1513.

[26] M. De Volder, S. Park, S. Tawfick, A. J. Hart, Nat. Commun. 2014.5, 5512.

[27] Z. F. Ren, Z. P. Huang, J. W. Xu, J. H. Wang, P. Bush, M. P. Siegal,P. N. Provencio, Science 1998, 282, 1105.

[28] C. T. Wirth, C. Zhang, G. Zhong, S. Hofmann, J. Robertson, ACS Nano 2009, 3, 3560.

[29] H. Sugime, S. Esconjauregui, J. Yang, L. D'Arsié, R. A. Oliver,S. Bhardwaj, C. Cepek, J. Robertson, Appl. Phys. Lett. 2013, 103,073116.

[30] P. Fayant, O. Girlanda, Y. Chebli, C.-É. Aubin, I. Villemure,A. Geitmann, The Plant Cell Online 2010, 22, 2579.

[31] S. J. Park, Carbon Nanotube Microarchitectures for Mechanical Metamaterials, Doctoral Dissertation, University of Michigan, Ann Arbor, MI, 2014.

[32] A. Y. Cao, P. L. Dickrell, W. G. Sawyer, M. N. Ghasemi-Nejhad,P. M. Ajayan, Science 2005, 310, 1307.

[33] M. R. Maschmann, G. J. Ehlert, S. J. Park, D. Mollenhauer,B. Maruyama, A. J. Hart, J. W. Baur, Adv. Funct. Mater. 2012, 22,4686.

[34] C. P. Deck, J. Flowers, G. S. B. McKee, K. Vecchio, J. Appl. Phys.2007, 101, 023512.

[35] M. R. Maschmann, G. J. Ehlert, S. Tawfi ck, A. J. Hart, J. W. Baur,Carbon 2014, 66, 377.

[36] S. Tawfi ck, Z. Zhao, M. Maschmann, A. Brieland-Shoultz ,M. De Volder, J. W. Baur, W. Lu, A.J. Hart, Langmuir 2013, 29,5190.

[37] G. Toth, J. Mäklin, N. Halonen, J. Palosaari, J. Juuti, H. Jantunen,K. Kordas, W. G. Sawyer, R. Vajtai, P. M. Ajayan, Adv. Mater. 2009,21, 2054.

[38] Y. Won, Y. Gao, M. A. Panzer, R. Xiang, S. Maruyama,T. W. Kenny, W. Cai, K. E. Goodson, Proc. Natl. Acad. Sci. 2013,110, 20426.

[39] A. J. Hart, A. H. Slocum, Nano Lett. 2006, 6, 1254.

[40] J. Choi, S. Pyo, D.-H. Baek, J.-I. Lee, J. Kim, Carbon 2014. 66, 126.

[41] F. V. De Blasio, Lethaia 2008, 41, 15.

[42] M. Bedewy, B. Farmer, A. J. Hart, ACS Nano 2014, 8, 5799.Received: March 31, 2016 Revised: April 27, 2016Published online: July 5, 2016